


Equilibrium magnetization of a quasispherical cluster of single-domain particles

Andrey A. Kuznetsov*

Institute of Continuous Media Mechanics UB RAS, Perm Federal Research Center UB RAS, 614013 Perm, Russia (Received 19 April 2018; revised manuscript received 12 September 2018; published 12 October 2018)

Equilibrium magnetization curve of a rigid finite-size spherical cluster of single-domain particles is investigated both numerically and analytically. The spatial distribution of particles within the cluster is random. Dipole-dipole interactions between particles are taken into account. The particles are monodisperse. It is shown, using the stochastic Landau-Lifshitz-Gilbert equation that the magnetization of such clusters is generally lower than predicted by the classical Langevin model. In a broad range of dipolar coupling parameters and particle volume fractions, the cluster magnetization in the weak field limit can be successfully described by the modified mean-field theory, which was originally proposed for the description of concentrated ferrofluids. In moderate and strong fields, the theory overestimates the cluster magnetization. However, predictions of the theory can be improved by adjusting the corresponding mean-field parameter. If magnetic anisotropy of particles is additionally taken into account and if the distribution of the particles' easy axes is random and uniform, then the cluster equilibrium response is even weaker. The decrease of the magnetization with increasing anisotropy constant is more pronounced at large applied fields. The phenomenological generalization of the modified mean-field theory, that correctly describes this effect for small coupling parameters, is proposed.

DOI: [10.1103/PhysRevB.98.144418](https://doi.org/10.1103/PhysRevB.98.144418)**I. INTRODUCTION**

Nano- and microsized assemblies of single-domain particles are of great interest in modern biotechnology and medicine. Prominent examples are composite magnetic microspheres (or “magnetic beads”) which consist of fine magnetic particles dispersed in or layered onto a spherical (usually polymer or silica) matrix [1,2]. The diameter of embedded particles can range from several to several dozen nanometers, and the characteristic size of microspheres themselves most commonly ranges from tenths to several microns. One of the most popular applications of magnetic microspheres is the magnetic cell separation—a technique that allows one to magnetically label cells of a specific type and then isolate them from a heterogeneous cell mixture using a gradient field [3,4]. Also microspheres can be used as magnetically controlled carriers for targeted drug delivery [5,6] and as force and torque transducers in magnetic tweezers designed to probe mechanical properties of biomolecules [7,8].

Another important class of objects is dense three-dimensional (3D) nanoclusters of single-domain particles which are sometimes referred to as “magnetic multicore nanoparticles” [9–11]. Such clusters are typically covered with a nonmagnetic protective coating and have a hydrodynamic diameter of 50–200 nm. Multicore nanoparticles can be thought of as intermediate between single-domain nanoparticles and magnetic microspheres [12]. From the viewpoint of cell separation, nanoclusters have some advantages over micrometer-sized beads: For example, they are more stable against sedimentation and have a better binding capacity due to a higher surface-area-to-volume ratio [4,13].

Multicore nanoparticles are considered to be perspective for magnetic hyperthermia treatment [14,15] and magnetic imaging [16,17]. Aside from their high biomedical potential, magnetic 3D nanoclusters are also interesting due to their presence in some types of ferrofluids [18,19]. It is known that suspended nanoclusters can significantly alter the fluid's magnetic, mass-transfer, and rheological properties [20,21].

For simplicity, it is sometimes assumed that microspheres and nanoclusters contain noninteracting and magnetically isotropic single-domain particles [7,20–22]. However, in recent years quasispherical rigid clusters of different sizes have been actively studied via numerical simulations [11,23–28], and it has been repeatedly demonstrated that interactions between embedded particles as well as their magnetic anisotropy can have a noticeable impact on the cluster static [11,23–25] and dynamic [25–28] magnetic properties. Particularly, in Refs. [11,25] the equilibrium magnetization curve of a quasispherical cluster of uniaxial particles was considered. Dipole-dipole interactions between particles were taken into account. It was demonstrated that for a monodisperse system with a uniform distribution of easy axes the magnetization is generally lower than predicted by the classical Langevin model and that both anisotropy and interactions contribute to the decrease of the cluster equilibrium response.

Though a number of simulation results are currently available, it can be useful to have an analytical model that links properties of particles inside a rigid 3D cluster with the system magnetization. For single-domain particles dispersed in a liquid matrix, many such models exist [29]. Among them the so-called “modified mean-field theory” (MMFT) remains one of the most widely used due to its simplicity and accuracy [30–32]. In Refs. [33,34] it was shown that MMFT also gives correct predictions for the initial susceptibility of magnetoisotropic particles randomly distributed in a solid

*kuznetsov.a@icmm.ru

matrix. Good agreement between simulations and MMFT was obtained for both the bulk system [33] and the finite spherical cluster [34]. The question of whether MMFT is applicable to clusters beyond the weak field limit, to the best of our knowledge, has not been addressed in the literature.

In this paper, the equilibrium magnetization curve of a rigid quasispherical cluster of uniaxial particles is studied via Langevin dynamics simulations. In contrast to recent works [11,25], special attention is paid to the effect of particle volume fraction on the cluster properties. The applicability of MMFT for the description of magnetic 3D clusters is tested. Possible ways to improve the agreement between the analytical model and simulations are discussed.

II. MODEL AND METHODS

A. Model formulation

Let us consider an ensemble of N identical spherical single-domain particles randomly distributed within a spherical volume of radius R . Positions of particles inside this volume are fixed; particle overlapping is not allowed. Each particle has a diameter d and a magnetic moment $\boldsymbol{\mu}$, which can rotate inside the particle; the corresponding unit vector is $\mathbf{e} = \boldsymbol{\mu}/\mu$. The magnitude of the magnetic moment is $\mu = M_s v$, where M_s is the saturation magnetization of the particle material, and $v = (\pi/6)d^3$ is the particle volume. Particles have uniaxial magnetic anisotropy, which is characterized by the anisotropy constant K and the easy axis unit vector \mathbf{n} . Each particle has its own fixed vector \mathbf{n} . The orientation distribution of easy axes is random and uniform. Particles interact with each other via dipole-dipole interactions. The described system is further referred to as the ‘‘cluster.’’ The cluster is immobilized inside a nonmagnetic medium and subjected to a uniform magnetic field \mathbf{H} (the corresponding unit vector is $\mathbf{h} = \mathbf{H}/H$). The total magnetic energy of the cluster is

$$U = U_Z + U_{\text{ani}} + U_{dd}, \quad (1)$$

$$U_Z = -\mu_0 \mu H \sum_{i=1}^N \mathbf{e}_i \cdot \mathbf{h}, \quad (2)$$

$$U_{\text{ani}} = -Kv \sum_{i=1}^N (\mathbf{e}_i \cdot \mathbf{n}_i)^2, \quad (3)$$

$$U_{dd} = -\frac{\mu_0 \mu^2}{4\pi d^3} \sum_{i=1}^N \sum_{j=i+1}^N \times \left[\frac{3(\mathbf{e}_i \cdot \mathbf{r}_{ij}^*)(\mathbf{e}_j \cdot \mathbf{r}_{ij}^*)}{r_{ij}^{*5}} - \frac{\mathbf{e}_i \cdot \mathbf{e}_j}{r_{ij}^{*3}} \right], \quad (4)$$

where U_Z is the Zeeman energy, U_{ani} is the magnetic anisotropy energy, U_{dd} is the dipole-dipole interaction energy, the summation in Eqs. (2–4) is over particles in the cluster, μ_0 is the magnetic constant, and $\mathbf{r}_{ij}^* = \mathbf{r}_{ij}/d$, \mathbf{r}_{ij} is the vector between centers of particles i and j .

At nonzero temperature T , the normalized magnetic moment of the cluster

$$\mathbf{m} = \frac{1}{N} \sum_{i=1}^N \mathbf{e}_i \quad (5)$$

is a random vector with fluctuating magnitude and direction. The equilibrium magnetization of the cluster can be determined as

$$M = \frac{1}{V} \left\| \left\langle \sum_{i=1}^N \boldsymbol{\mu}_i \right\rangle \right\| = M_\infty \|\langle \mathbf{m} \rangle\| = M_\infty \langle m_h \rangle, \quad (6)$$

where $V = (4\pi/3)R^3$ is the cluster volume, $M_\infty = \mu N/V$ is the saturation magnetization of the cluster, $m_h = \mathbf{m} \cdot \mathbf{h}$ is the projection of the cluster moment on the field direction, and angle brackets denote a mean value. Equilibrium magnetization of the cluster is determined by several dimensionless parameters. First of all, this is the so-called Langevin parameter

$$\xi = \frac{\mu_0 \mu H}{k_B T}, \quad (7)$$

which is the characteristic ratio between Zeeman and thermal energies; k_B is the Boltzmann constant. The dependence of $\langle m_h \rangle$ on ξ can be considered as the cluster magnetization curve. Finding this dependency is the main focus of this work. Other key parameters are the anisotropy parameter

$$\sigma = \frac{Kv}{k_B T}, \quad (8)$$

the dipolar coupling parameter

$$\lambda = \frac{\mu_0 \mu^2}{4\pi d^3 k_B T}, \quad (9)$$

and the particle volume fraction

$$\varphi = \frac{vN}{V}. \quad (10)$$

Let us make some estimates based on material parameters for magnetic solids given in Ref. [35]. First of all, it should be noted that dipolar coupling and anisotropy parameters are not independent variables for particles of a given material, $\sigma/\lambda = (24/\mu_0)K/M_s^2$ (here we neglect the difference between the particle diameter and the diameter of its magnetic core). For cobalt ferrite ($M_s = 425 \text{ kA m}^{-1}$, $K = 180\text{--}200 \text{ kJ m}^{-3}$), $\sigma/\lambda \simeq 20$; for magnetite ($M_s = 446 \text{ kA m}^{-1}$, $K = 23\text{--}41 \text{ kJ m}^{-3}$), $\sigma/\lambda = 2\text{--}4$. Since iron oxide nanoparticles are more common in biomedical applications [25], here we confine ourselves to the cases when σ and λ are comparable. At $T = 300 \text{ K}$, magnetite nanoparticles with $d = 10 \text{ nm}$ have $\lambda \simeq 1.3$, and $\xi = 1$ corresponds to $H \simeq 14 \text{ kA m}^{-1}$. The same nanoparticles with $d = 13 \text{ nm}$ have $\lambda \simeq 2.9$, and $\xi = 1$ corresponds to $H \simeq 6.4 \text{ kA m}^{-1}$. In this work, the following ranges of control parameters are considered: $\xi \leq 10$, $\sigma \leq 10$, $\lambda \leq 3$, $\varphi \leq 0.3$, and $N = 10^2\text{--}10^3$.

B. Limiting case of noninteracting particles

Equilibrium magnetic properties of noninteracting uniaxial particles in a solid matrix were previously discussed in

Refs. [36–41]. Let us briefly recall some results of these works. If interactions between particles can be neglected, i.e., in the limiting cases $\varphi \ll 1$ or $\lambda \ll 1$, the equilibrium magnetization can be derived within the one-particle approximation. The ratio between magnetic and thermal energies for an isolated particle is usually written as

$$\frac{u}{k_B T} = -\xi \cos \omega + \sigma \sin^2 \vartheta, \quad (11)$$

where ω is the angle between the particle moment and the field, and ϑ is the angle between the moment and the easy axis. The system magnetization is determined by the average value of $\cos \omega = \mathbf{e} \cdot \mathbf{h}$, which can be found as

$$\langle \cos \omega \rangle = \frac{1}{Z} \frac{\partial Z}{\partial \xi}, \quad (12)$$

where Z is the partition function of the particle. If particles have negligible magnetic anisotropy ($\sigma \ll 1$), the partition function is

$$Z = \frac{1}{2} \int_0^\pi \exp(\xi \cos \omega) \sin \omega d\omega = \frac{\sinh \xi}{\xi}, \quad (13)$$

which, in combination with Eq. (12), gives the well-known Langevin magnetization:

$$\langle m_h \rangle = \langle \cos \omega \rangle = \mathcal{L}(\xi), \quad (14)$$

where $\mathcal{L}(\xi) \equiv \coth \xi - 1/\xi$ is the Langevin function. For uniaxial particles, the partition function and its first derivative can be written in the following single-integral forms [41]:

$$Z = \mathcal{J}_0(\xi, \sigma, \psi) \equiv \int_0^{\pi/2} \exp(-\sigma \sin^2 \vartheta) \cosh(\xi \cos \vartheta \cos \psi) \times I_0(\xi \sin \vartheta \sin \psi) \sin \vartheta d\vartheta, \quad (15)$$

$$\begin{aligned} \frac{\partial Z}{\partial \xi} &= \mathcal{J}_1(\xi, \sigma, \psi) \\ &\equiv \int_0^{\pi/2} \exp(-\sigma \sin^2 \vartheta) [\cosh(\xi \cos \vartheta \cos \psi) \\ &\quad \times I_1(\xi \sin \vartheta \sin \psi) \sin \vartheta \sin \psi + \sinh(\xi \cos \vartheta \cos \psi) \\ &\quad \times I_0(\xi \sin \vartheta \sin \psi) \cos \vartheta \cos \psi] \sin \vartheta d\vartheta, \end{aligned} \quad (16)$$

where ψ is the angle between the field and the easy axis ($\cos \psi = \mathbf{n} \cdot \mathbf{h}$), I_0 and I_1 are the modified Bessel functions of the first kind of order zero and one, correspondingly. Thus, for an arbitrary particle with a given easy axis orientation ψ , the following expression is valid:

$$\langle \cos \omega \rangle = \frac{\mathcal{J}_1(\xi, \sigma, \psi)}{\mathcal{J}_0(\xi, \sigma, \psi)}. \quad (17)$$

If particles in the system have different orientations of easy axes, then one has to average Eq. (17) over all presented values of ψ to obtain the net magnetization. It was demonstrated in Ref. [37] that the distribution of easy axes (the system ‘‘orientation texture’’) effects the magnetization curve significantly. For the special case of a random uniform distribution, the magnetization is [39,41]

$$\langle m_h \rangle = \mathcal{L}_{\text{ani}}(\xi, \sigma) \equiv \int_0^{\pi/2} \frac{\mathcal{J}_1(\xi, \sigma, \psi)}{\mathcal{J}_0(\xi, \sigma, \psi)} \sin \psi d\psi. \quad (18)$$

The integral Eq. (18) is denoted here as $\mathcal{L}_{\text{ani}}(\xi, \sigma)$. This function can be considered as a generalization of the standard Langevin function for the case of solid dispersions with random orientation texture. In the limit of negligible anisotropy, two functions coincide, i.e., $\mathcal{L}_{\text{ani}}(\xi, 0) = \mathcal{L}(\xi)$. For finite nonzero values of ξ and σ , $\mathcal{L}_{\text{ani}}(\xi, \sigma) < \mathcal{L}(\xi)$ [37]. However, the zero-field slope of the magnetization curve (the initial magnetic susceptibility χ) does not depend on σ [36,38]:

$$\begin{aligned} \chi &= \frac{M}{H} \Big|_{H \rightarrow 0} = \frac{\mu_0 \mu^2 \varphi}{v k_B T} \left(\frac{\mathcal{L}_{\text{ani}}(\xi, \sigma)}{\xi} \Big|_{\xi \rightarrow 0} \right) \\ &= \frac{\mu_0 \mu^2 \varphi}{v k_B T} \left(\frac{\mathcal{L}(\xi)}{\xi} \Big|_{\xi \rightarrow 0} \right) = 3\chi_L \left(\frac{\mathcal{L}(\xi)}{\xi} \Big|_{\xi \rightarrow 0} \right) = \chi_L, \end{aligned} \quad (19)$$

where $\chi_L = \mu_0 \mu^2 \varphi / 3v k_B T = 8\lambda \varphi$ is the so-called Langevin susceptibility. For infinite anisotropy $\sigma = \infty$ and finite values of ξ , magnetic moments of particles can be considered as Ising-like spins with only two available states $\vartheta = 0$ and $\vartheta = \pi$ [40]. The magnetization in this asymptotic limit is given by [41]

$$\mathcal{L}_{\text{ani}}(\xi, \infty) = \int_0^{\pi/2} \cos \psi \tanh(\xi \cos \psi) \sin \psi d\psi. \quad (20)$$

C. Dipole-dipole interactions and modified mean-field theory

When one considers a body homogeneously filled with particles interacting via long-range dipole-dipole interactions, one of the main things that should be taken into account is the demagnetizing field. If a magnetizable body is placed in a uniform magnetic field \mathbf{H} , then the field inside the body \mathbf{H}_{int} does not coincide with \mathbf{H} in the general case. The difference between \mathbf{H} and \mathbf{H}_{int} is known as the demagnetizing field; it is created by the surface divergence of the body’s own magnetization \mathbf{M} [42]. For an arbitrary shaped body, demagnetizing fields can have a complex spatial distribution. But for the special case of an ellipsoid, the demagnetizing field is uniform. If \mathbf{H} lies along one of the principal axes of a magnetizable ellipsoid, then \mathbf{H}_{int} and \mathbf{M} also lie along this direction. Magnitudes of these vectors are connected as

$$H_{\text{int}} = H - \kappa M, \quad (21)$$

where $0 \leq \kappa \leq 1$ is the demagnetizing factor of the ellipsoid along the chosen axis. The factor κ depends only on the shape of the ellipsoid and not on its size. For an infinitely elongated (needlelike) ellipsoid parallel to the field, $\kappa = 0$, and for a sphere it is $\kappa = 1/3$.

Now let us consider a needlelike body with $H = H_{\text{int}}$ ($\kappa = 0$), filled with interacting magnetoisotropic particles ($\sigma = 0$). Even in this case, the equilibrium magnetic response cannot be described by the Langevin model. A possible way to expand the model is the well-known Weiss mean-field theory. According to it, an effective magnetic field acting locally on an arbitrary particle consists of the applied field H and an additional term which describes the impact of the particle surroundings. This term is proportional to the system magnetization M ; the proportionality factor is normally equal to the Lorentz value $1/3$ [43]. The system magnetization is then given by

$$M = M_L(H + M/3), \quad (22)$$

where $M_L(H) \equiv M_\infty \mathcal{L}(\mu_0 \mu H / k_B T)$. However, Eq. (22) is known to overestimate the effect of dipole-dipole interactions on concentrated assemblies of single-domain particles. Particularly, the Weiss theory predicts a spontaneous transition into an orientationally ordered “ferromagnetic” state at $\chi_L = 3$ [44,45], but such a transition has not been observed experimentally. Some more advanced theories and numerical simulations indicate the possibility of the transition both for liquid [46] and solid [47] matrices, but corresponding critical values of χ_L are significantly larger than predicted by the Weiss theory. In Ref. [30] the following heuristic modification of the mean-field theory was proposed for dispersions of single-domain particles in a liquid matrix (i.e., for ferrofluids):

$$M = M_L(H + M_L(H)/3). \quad (23)$$

In this expression, the impact of the system on an arbitrary particle is described not by the system actual magnetization M but by the magnetization the system would have in the absence of interactions, i.e., by $M_L(H)$. The statistical-mechanical approach developed in Ref. [31] subsequently justified the validity of the heuristic formula Eq. (23). Moreover, the authors of Ref. [31] suggested its refined version that reads

$$M = M_L \left(H + \frac{M_L(H)}{3} + \frac{M_L(H)}{144} \frac{dM_L(H)}{dH} \right). \quad (24)$$

Equations (23) and (24) are now known as the first- and second-order modified mean-field theories, correspondingly (MMFT1 and MMFT2). At small and moderate values of λ and φ , they are both in good agreement with experimental and numerical results on ferrofluid magnetization, though MMFT2 has a wider range of applicability [32]. However, MMFTs assume a homogeneous distribution of particles in the system and hence fail to describe an enhanced magnetic response at strong coupling $\lambda \geq 3$, which is due to the formation of chainlike aggregates [48]. The applicability of MMFTs for solid magnetic dispersions, where the formation of aggregates is forbidden, was numerically investigated in Refs. [33,34]. Only the initial magnetic susceptibility of the solid system was considered. According to Ref. [33], MMFT1 describes χ well for $\lambda \leq 3$ and $\varphi \leq 0.25$, while MMFT2 slightly overestimates the susceptibility. The applicability of MMFT for solid systems at nonzero fields is to be tested. Using previously defined dimensionless parameters, Eqs. (23) and (24) can be rewritten in the form

$$\langle m_h \rangle = \mathcal{L}(\xi + C_{mf}(\xi) \mathcal{L}(\xi)), \quad (25)$$

where C_{mf} is the mean-field parameter, which can depend on the applied field in the general case. For MMFT1:

$$C_{mf} = \chi_L, \quad (26)$$

for MMFT2:

$$C_{mf}(\xi) = \chi_L \left(1 + \frac{\chi_L}{16} \frac{d\mathcal{L}(\xi)}{d\xi} \right). \quad (27)$$

For a body with $\kappa \neq 0$, H in magnetization expressions must be replaced by H_{int} . For a sphere, the magnetization curve can

be then obtained in the following parametric form:

$$\langle m_h \rangle = \mathcal{L}(\xi_{\text{int}} + C_{mf}(\xi_{\text{int}}) \mathcal{L}(\xi_{\text{int}})), \quad (28)$$

$$\xi = \xi_{\text{int}} + \chi_L \langle m_h \rangle, \quad (29)$$

where $\xi_{\text{int}} = \mu_0 \mu H_{\text{int}} / k_B T$ is the parameter ($0 \leq \xi_{\text{int}} < \infty$); Eq. (29) corresponds to Eq. (21) with $\kappa = 1/3$.

To describe the cluster of interacting uniaxial particles, we propose here the following phenomenological generalization of Eq. (28), where both Langevin functions are replaced by \mathcal{L}_{ani} :

$$\langle m_h \rangle = \mathcal{L}_{\text{ani}}(\xi_{\text{int}} + C_{mf}(\xi_{\text{int}}) \mathcal{L}_{\text{ani}}(\xi_{\text{int}}, \sigma), \sigma), \quad (30)$$

The replacement of the first Langevin function ensures the correct behavior in the limit of noninteracting particles ($\xi_{\text{int}} = \xi$, $C_{mf} = 0$). As for the second replacement, we here speculate that the impact of a randomly textured solid dispersion on an arbitrary particle can be described by the mean-field term proportional to \mathcal{L}_{ani} , just like the impact of a system of magnetoisotropic particles is described by \mathcal{L} in MMFT. A suitable choice of the function $C_{mf} = C_{mf}(\xi)$ in Eq. (30) is discussed in Sec. III C.

D. Langevin dynamics simulation

To check the accuracy of the described models, the Langevin dynamics simulation is used. The Langevin equation that describes the magnetodynamics of a single-domain particle is the stochastic Landau-Lifshitz-Gilbert equation [25,49]. For the i th particle of the simulated cluster it reads

$$\frac{d\boldsymbol{\mu}_i}{dt} = -\gamma [\boldsymbol{\mu}_i \times \mathbf{H}_i^{\text{tot}}] - \frac{\gamma\alpha}{\mu} [\boldsymbol{\mu}_i \times [\boldsymbol{\mu}_i \times \mathbf{H}_i^{\text{tot}}]], \quad (31)$$

where $\gamma = \gamma_0 / (1 + \alpha^2)$, γ_0 is the gyromagnetic ratio (in meters per ampere per second), α is the dimensionless damping constant, $\mathbf{H}_i^{\text{tot}} = \mathbf{H}_i^{\text{det}} + \mathbf{H}_i^{\text{fl}}$, $\mathbf{H}_i^{\text{det}} = -(\partial U / \partial \boldsymbol{\mu}_i) / \mu_0$ is the total deterministic field acting on the particle, and \mathbf{H}_i^{fl} is the fluctuating thermal field. $\mathbf{H}_i^{\text{fl}}(t)$ is a Gaussian stochastic process with the following statistical properties:

$$\langle \mathbf{H}_{i,k}^{\text{fl}}(t) \rangle = 0, \quad \langle \mathbf{H}_{i,k}^{\text{fl}}(t_1) \mathbf{H}_{j,l}^{\text{fl}}(t_2) \rangle = 2D \delta_{ij} \delta_{kl} \delta(t_1 - t_2), \quad (32)$$

where k and l are Cartesian indices, $D = \alpha k_B T / \mu_0 \mu \gamma (1 + \alpha^2)$. Equation (31) can be rewritten in the dimensionless form:

$$\frac{d\mathbf{e}_i}{dt^*} = -\frac{1}{2\alpha} [\mathbf{e}_i \times \boldsymbol{\xi}_i^{\text{tot}}] - \frac{1}{2} [\mathbf{e}_i \times [\mathbf{e}_i \times \boldsymbol{\xi}_i^{\text{tot}}]], \quad (33)$$

where the $t^* = t / \tau_D$ is the dimensionless time, $\tau_D = \mu_0 \mu / 2\alpha \gamma k_B T$ is the characteristic time scale of the rotary diffusion of the magnetic moment, $\boldsymbol{\xi}_i^{\text{tot}} = \mu_0 \mu \mathbf{H}_i^{\text{tot}} / k_B T = \boldsymbol{\xi}_i^{\text{det}} + \boldsymbol{\xi}_i^{\text{fl}}$,

$$\boldsymbol{\xi}_i^{\text{det}} = \xi \mathbf{h} + 2\sigma (\mathbf{e}_i \cdot \mathbf{n}_i) \mathbf{n}_i + \lambda \sum_{j \neq i}^N \left[\frac{3\mathbf{r}_{ij}^* (\mathbf{e}_j \cdot \mathbf{r}_{ij}^*)}{r_{ij}^{*5}} - \frac{\mathbf{e}_j}{r_{ij}^{*3}} \right], \quad (34)$$

$$\langle \boldsymbol{\xi}_{i,k}^{\text{fl}}(t^*) \rangle = 0, \quad \langle \boldsymbol{\xi}_{i,k}^{\text{fl}}(t_1^*) \boldsymbol{\xi}_{j,l}^{\text{fl}}(t_2^*) \rangle = \frac{4\alpha^2}{1 + \alpha^2} \delta_{ij} \delta_{kl} \delta(t_1^* - t_2^*). \quad (35)$$

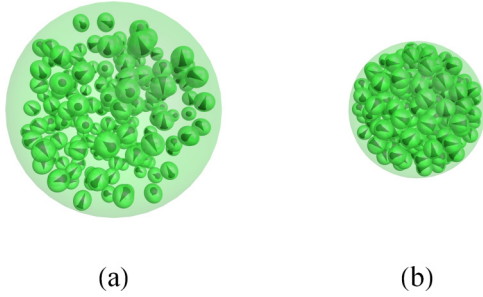


FIG. 1. Examples of rigid clusters used in simulations, $\lambda = \sigma = \xi = 0$, $N = 200$. (a) $\varphi = 0.1$, $R \approx 6.3d$, (b) $\varphi = 0.3$, $R \approx 4.4d$.

The input parameters of the simulation are N , φ , λ , ξ , and σ . The cluster at given N and φ is generated as follows. The i th particle is randomly placed inside a cube with a side length of $2R$ ($1 \leq i \leq N$, $R = (d/2)\sqrt[3]{N/\varphi}$). If after this the particle is outside of the sphere of radius R or if it overlaps with previously placed particles (i.e., with particles $j < i$), the position is rejected and the new position is generated. This is repeated until a suitable position is found. Then \mathbf{n}_i and the initial state of \mathbf{e}_i are chosen at random. Then the state of the particle $i + 1$ is generated according to the same rules. Examples of clusters with $N = 200$ and different volume fractions are shown in Fig. 1.

After the cluster is generated, the Heun scheme [49] is used for the numerical integration of Eq. (33), the damping constant is $\alpha = 0.2$, and the integration time step is $\Delta t^* = 0.002$, unless otherwise specified. Dipole-dipole interaction fields between particles in the cluster are calculated without truncation; no periodic boundary conditions (PBCs) are applied. The main result of the simulation is the average normalized magnetization of the cluster $\langle m_h \rangle$. In the case $\sigma = 0$, the sampling of m_h values typically starts after the time $t^* = 100$, but for $\sigma > 0$ a much longer equilibration period might be required. This issue is discussed in Sec. III C. For each particular set of input parameters, the magnetization value is additionally averaged over several independent realizations of the cluster. However, the results for different realizations are proved to be close, so their number is not large. Most of the magnetization curves presented below are averaged over ten realizations of the cluster.

In addition to clusters, this paper also briefly discusses the equilibrium magnetization of a bulk solid dispersion of magnetic nanoparticles (see Sec. III A). The input simulation parameters in this case are the same as for the cluster. The simulation cell is a cube with a side length of $L = d\sqrt[3]{\pi N/6\varphi}$. PBCs are applied in all three directions. The dipolar fields in the system are calculated using the standard Ewald summation with “metallic” boundary conditions. This technique ensures a proper handling of long-range effects of dipole-dipole interactions. In its “metallic” version the internal field in the simulation box coincides exactly with the applied field. A detailed description of the technique is available in Refs. [33,50].

III. RESULTS AND DISCUSSION

A. Magnetically isotropic particles in a bulk solid matrix

Before moving on to the main object of our interest, i.e., the finite-size magnetic cluster, it may be useful to consider the

equilibrium magnetization of a bulk solid matrix filled with magnetic nanoparticles and to test the applicability of MMFTs for such a system. In numerical simulations we model bulk in a standard way by applying PBCs to a cubic simulation cell. First of all, the usage of PBCs minimizes possible size effects that may arise in the simulation of the cluster. Besides, we use the “metallic” version of the Ewald summation technique to calculate dipole-dipole interactions. This method assumes that the large system formed by the simulation cell and its PBC images is surrounded by a medium with infinite magnetic permeability [33]. In this case, $\xi = \xi_{\text{int}}$ and the system magnetic behavior is the same as that of an elongated cylindrical sample. So, the demagnetizing fields, which are inevitable for the quasispherical cluster in a nonmagnetic medium, are now absent. In this section, we only consider the case $\sigma = 0$.

Static magnetization curves of bulk systems with different values of φ and λ are given in Fig. 2. To emphasize the effect of interparticle interactions on the equilibrium magnetic properties, we also give in Figs. 2(c) and 2(d) the differences between the system actual magnetization and the Langevin function. Symbols denote values obtained after averaging over ten independent realizations of the simulated system; error bars here and below denote corresponding 95% confidence intervals. It is seen that MMFT1 [Eqs. (25) and (26)] and MMFT2 [Eqs. (25) and (27)] give good agreement with the simulation data in the weak field range ($\xi < 1$). In Fig. 3 the system initial susceptibility χ is plotted vs the Langevin susceptibility χ_L . According to MMFT1, the susceptibility is [31]

$$\chi = \chi_L(1 + \chi_L/3), \quad (36)$$

and according to MMFT2, it is

$$\chi = \chi_L(1 + \chi_L/3 + \chi_L^2/144). \quad (37)$$

The susceptibility of the simulated system is estimated simply as $\chi = 3\chi_L\langle m_h(\xi = 0.05) \rangle/0.05$. For $\lambda \leq 3$ and $\varphi \leq 0.25$, MMFT1 describes calculated susceptibilities well, which agrees with the results of Ref. [33]. At $\lambda = 3$ and $\varphi > 0.25$ (which corresponds to $\chi_L > 6$ for $\lambda = 3$), the susceptibility is seemingly better described by MMFT2. In Ref. [33] the behavior of solid systems at $\varphi > 0.25$ was not investigated. More conspicuous deviations between MMFT1 and the simulation results are observed in Fig. 2 at moderate and strong fields. The theory clearly overestimates the simulation results at $\xi \geq 1$ for all inspected values of interaction parameters. The deviation is larger for higher λ . As seen in Figs. 2(c) and 2(d), the magnetization of a bulk solid system at moderate and large ξ is closer to the Langevin curve than MMFT1 predicts. Despite this fact, the deviation between the simulation results and the Langevin model is still significant. The maximum difference between $\langle m_h \rangle$ and $\mathcal{L}(\xi)$ is observed at $\xi \sim 1$. For $\lambda = 3$ and $\varphi = 0.3$, it reaches ≈ 0.28 . In other words, the difference between the nonreduced magnetization M and M_L is $\approx 28\%$ of the system saturation magnetization M_∞ . As ξ increases, the calculated magnetization approaches the Langevin curve much faster than it should according to MMFT1. For one of the investigated parameter sets ($\lambda = 3$, $\varphi = 0.1$), the calculated values of $\langle m_h \rangle$ are even smaller than $\mathcal{L}(\xi)$ at $\xi \gtrsim 7$ [though the maximum value of the difference $M_L - M$ is less than one percent of M_∞ as seen in the inset of Fig. 2(d)]. As

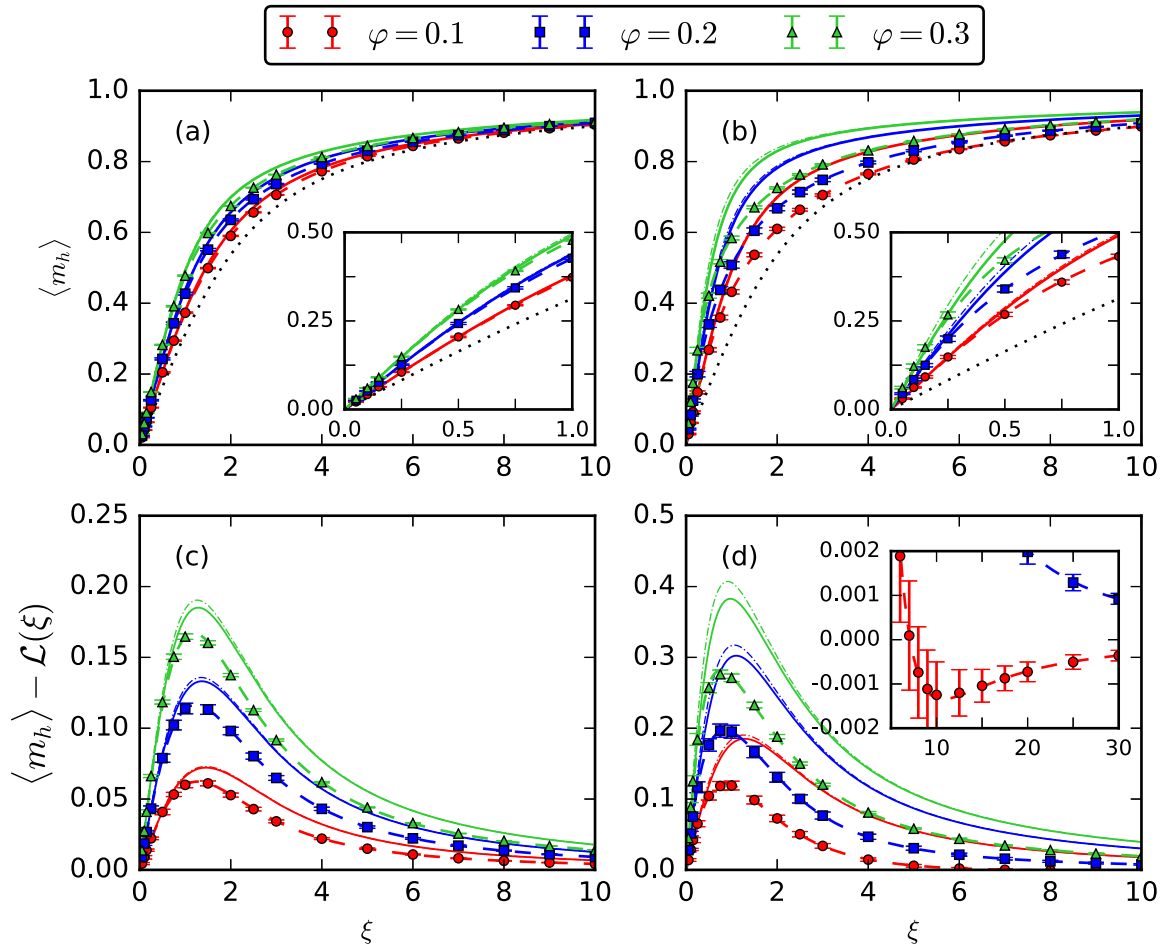


FIG. 2. Equilibrium magnetization curves of bulk solid systems with $H = H_{\text{int}}$ and $\sigma = 0$. $\lambda = 1$ (a) and 3 (b). Symbols are the simulation results for $N = 1000$; different combinations of symbols and colors correspond to different particle volume fractions φ (see legend). Solid curves are MMFT1 results for the same values of φ [Eqs. (25) and (26)], dot-dashed lines are MMFT2 results [Eqs. (25) and (27)], dashed curves are from the analytical model given by Eqs. (25) and (39), dotted lines are from the Langevin model [Eq. (14)]. Insets in (a) and (b) zoom on the weak field region. Figures (c) and (d) show differences between the magnetization values shown in (a), (b), and the Langevin function; (c) corresponds to (a) (i.e., to $\lambda = 1$) and (d) corresponds to (b) (i.e., to $\lambda = 3$). The inset in (d) shows values of $\langle m_h \rangle - \mathcal{L}(\xi)$ in the strong field region.

for MMFT2, it overestimates simulation data at large fields even stronger than MMFT1. Such overestimation was not observed in ferrofluid simulations—in the strong coupling case ($\lambda > 2$) and at $\xi \geq 1$ the ferrofluid magnetization is either slightly lower than predictions of MMFTs (at high concentrations) or greatly exceeds it (at low concentrations) [33]. A possible explanation is as follows. According to MMFTs, the effective field H_{eff} acting on an arbitrary particle i is always larger than the applied field H , and the difference $H_{\text{eff}} - H$ becomes larger with increasing H . Within this theory, dipole-dipole interactions between the i th particle and its surroundings, on average, always help the particle to align with the applied field. Based on our simulation results, this is true for solid dispersions of magnetic particles in the weak field limit. But at large fields the situation can become complicated due to the anisotropic nature of dipole-dipole interactions. Let us choose a Cartesian coordinate system so that its center coincides with the center of the i th particle and the Z axis coincides with the applied field direction \mathbf{h} . If ξ is large enough, magnetic moments of all particles

in the system are predominantly directed along the Z axis. If the particle j with $\mathbf{e}_j \parallel \mathbf{h}$ is placed somewhere on the Z axis, then the dipolar field created by this particle at the location of the i th particle is co-directed with \mathbf{h} . However, if the j th particle is placed in the XY plane, then its dipolar field at the i th particle location is directed opposite to \mathbf{h} . In ferrofluids, the anisotropy of dipole-dipole interactions results in the field-induced anisotropy of the pair distribution function [51]. In a liquid matrix, the probability to find the j th particle on the Z axis in close contact with the particle i becomes higher with increasing ξ . Two co-directed particles with $\mathbf{r}_{ij} \parallel \mathbf{h}$ tend to attract each other and form an energetically favorable “head-to-tail” configuration. This effect is noticeable even at relatively low dipolar coupling $\lambda \simeq 1$. At large λ , it transforms in the well-known formation of chainlike aggregates. On the contrary, the probability to find the j th particle in the plane XY in close contact with the particle i decreases with increasing ξ . Two co-directed particles with $\mathbf{r}_{ij} \perp \mathbf{h}$ tend to repel each other. So, as the field increases, magnetic particles in a liquid matrix tend to redistribute themselves so that the

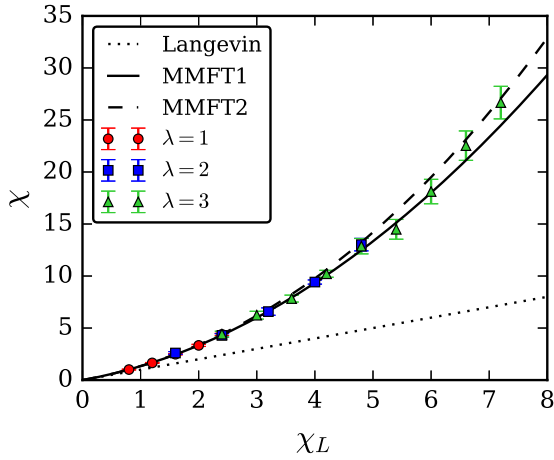


FIG. 3. Initial magnetic susceptibility χ of magnetoisotropic particles embedded in a bulk solid matrix vs the Langevin susceptibility χ_L . Symbols are the simulation results for $N = 1000$; different symbols correspond to different values of the dipolar coupling constant λ (see legend). Dotted line corresponds to the Langevin model ($\chi = \chi_L$), solid line is from MMFT1 [Eq. (36)], dashed line is from MMFT2 [Eq. (37)].

local surroundings of the i th particle is more likely to contain particles that favor the orientation of e_i along \mathbf{h} . But in our case, the isotropic spatial distribution of particles is frozen. So, at large applied fields the i th particle is surrounded both by particles that help it to align with the field and by particles that interfere with such behavior. It seems probable that, as the average result of such competition, the effective field H_{eff} acting on the i th particle in a solid matrix with increasing H becomes smaller than the corresponding effective field in a liquid matrix. As the inset in Fig. 2(d) suggests, in some cases H_{eff} can even become slightly smaller than H . In Eq. (25) the effect of the particle surroundings is controlled by the mean-field parameter C_{mf} . In order to correctly describe the observed behavior of a solid dispersion, this parameter should become significantly lower than the standard MMFT1 value χ_L at large fields. Figure 4 shows the values of C_{mf} extracted from the simulation data using the expression

$$C_{mf}(\xi) = \frac{\mathcal{L}^{-1}(\langle m_h \rangle) - \xi}{\mathcal{L}(\xi)}, \quad (38)$$

where $\mathcal{L}^{-1}(x)$ is the inverse Langevin function (its values were obtained numerically). The mean-field parameter in the figure is divided by χ_L . It is seen that at $\xi \ll 1$ $C_{mf}/\chi_L \gtrsim 1$, but it becomes lower at large fields, just as expected. At $\xi \gtrsim 2$, values of C_{mf}/χ_L decrease relatively fast; at a given λ they are almost the same for different volume fractions. For $\xi > 2$, the quantity C_{mf}/χ_L seemingly begins to reach a plateau. The values of C_{mf}/χ_L at large fields for different combinations of λ and φ do not coincide. Particularly, they are very different for $\lambda = 1$ and $\varphi = 0.3$ and for $\lambda = 3$ and $\varphi = 0.1$, despite the fact that the Langevin susceptibility is the same in both cases ($\chi_L = 2.4$). For $\lambda = 3$ and $\varphi = 0.1$, the mean-field parameter at large ξ becomes negative, which is why $\langle m_h \rangle$ at these parameters becomes smaller than $\mathcal{L}(\xi)$. At large ξ , values of C_{mf}/χ_L increase with increasing φ if λ is fixed. The increase

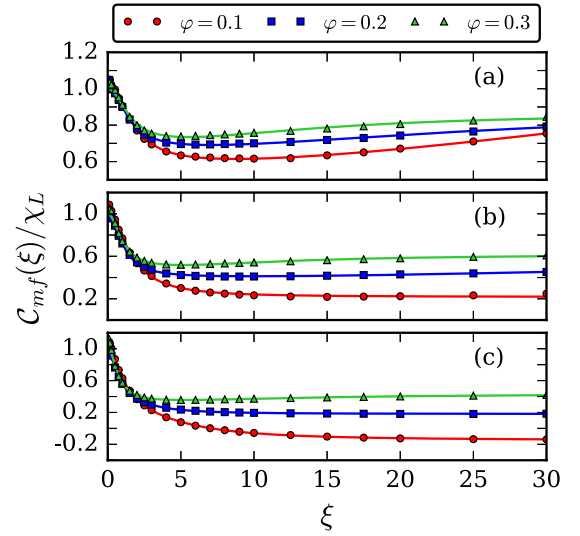


FIG. 4. Applied field dependencies of the mean-field parameter for bulk solid systems of magnetoisotropic particles. $\lambda = 1$ (a), 2 (b), and 3 (c). Symbols are simulation results for $N = 1000$; different symbols correspond to different volume fractions (see legend). Solid lines are from the approximation Eq. (39).

in λ at a fixed volume fraction has the opposite effect—in this case C_{mf}/χ_L decreases. To be able to check whether or not the mean-field parameters obtained for bulk systems are applicable for the description of clusters at large fields, we approximated the dependencies presented in Fig. 4 with the expression

$$C_{mf}(\xi) = \chi_L \frac{1 + a_2 \xi^2 + a_4 \xi^4}{1 + b_2 \xi^2 + b_4 \xi^4}. \quad (39)$$

Equation (39) contains only even powers of ξ , so that Eq. (25) remains an odd function of the magnetic field. Coefficients a_2 , a_4 , b_2 , and b_4 were separately determined for each investigated combination of λ and φ using nonlinear least squares fitting. The calculated values are given in Table I. The approximations are valid at least up to $\xi = 30$.

B. Cluster of magnetically isotropic particles

One of our main concerns regarding simulations of the cluster were possible finite-size effects. In Ref. [52] it was

TABLE I. Fitting parameters of Eq. (39) for different dipolar coupling constants and particle volume fractions.

λ	φ	a_2	a_4	b_2	b_4
1	0.1	0.165553	0.000119	0.286021	0.000083
	0.2	0.294838	0.000583	0.444823	0.000662
	0.3	0.289164	0.001879	0.417613	0.002166
2	0.1	0.312283	0.015637	0.629365	0.071964
	0.2	0.340067	0.000143	0.854058	0.000202
	0.3	0.429252	0.004477	0.901514	0.007247
3	0.1	0.217007	-0.004704	0.864708	0.031570
	0.2	1.632664	0.128207	3.249253	0.708223
	0.3	0.555831	0.004696	1.689059	0.010885

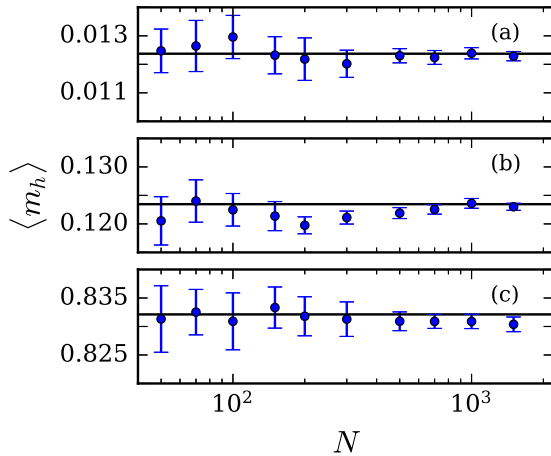


FIG. 5. Normalized equilibrium magnetization of the cluster vs the number of particles it contains. $\lambda = 3$, $\varphi = 0.3$, and $\sigma = 0$. $\xi = 0.1$ (a), 1 (b), 10 (c). Symbols are simulation results. Horizontal lines correspond to predictions of the analytical model given by Eqs. (28) and (39).

shown that properties of finite spherical containers with ferrofluid depend heavily on the system size in the case of strong dipolar coupling. Equilibrium magnetization of systems with $N \sim 10^2$ – 10^3 proved to be much smaller than corresponding thermodynamic limit values. Magnetization values of rigid clusters with $\sigma = 0$ are shown in Fig. 5 as a function of the particle number N at different values of ξ . These data are calculated for $\lambda = 3$ and $\varphi = 0.3$, i.e., for the largest values of interaction parameters considered in this work. Luckily, the results do not indicate strong size dependencies for rigid quas spherical clusters. This gives hope that approximations Eq. (39) derived for a bulk system will work for small clusters as well.

Static magnetization curves for clusters with $\sigma = 0$ and $\lambda = 3$ are given in Fig. 6. Due to the presence of demagnetizing fields, the effect of interactions is the opposite of what was observed in the previous section. Magnetization of the cluster is now always smaller than what the Langevin model predicts and the cluster equilibrium response is weaker the higher the volume fraction φ . Just like in the bulk case, MMFT1 [which is now given by Eqs. (26) and (28)] provides an accurate description of the magnetization curve initial slope, but overestimates the simulation results at strong fields ($\xi \gtrsim 2$). MMFT2 [Eqs. (27) and (28)] again gives larger magnetization values than MMFT1, but it should be noted that the difference between two theories is much less pronounced than in the bulk case. The combination of Eq. (28) and approximation Eq. (39) with fitting parameters taken from Table I accurately describes the cluster magnetization at all investigated values of φ and ξ . The foregoing is also true for smaller coupling parameters, but the difference between the cluster magnetization and the Langevin function in this case is much less distinguishable. For example, at $\lambda = 1$ and $\varphi = 0.3$, the maximum value of $\mathcal{L}(\xi) - \langle m_h \rangle$ is ≈ 0.09 . For $\lambda = 3$ and $\varphi = 0.3$, the difference $\mathcal{L}(\xi) - \langle m_h \rangle$ can become larger than 0.3 (which is seen in the inset of Fig. 6).

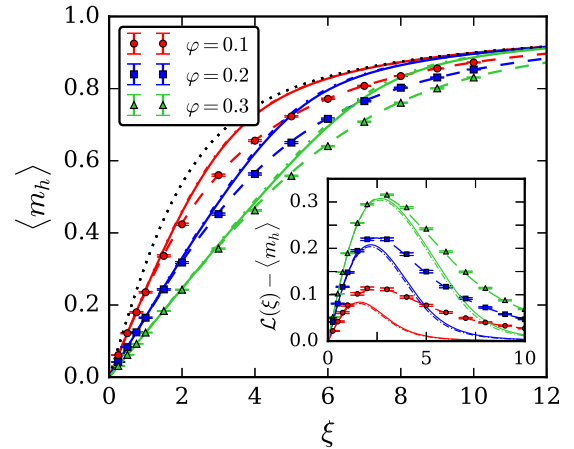


FIG. 6. Equilibrium magnetization curves of clusters with $\sigma = 0$ and $\lambda = 3$. Symbols are simulation results for $N = 1000$; different combinations of symbols and colors correspond to different volume fractions (see legend). Solid curves are prediction of MMFT1 [Eqs. (26) and (28)] for the same volume fractions; dot-dashed curves are predictions of MMFT2 [Eqs. (27) and (28)]. Dashed lines are from the analytical model given by Eqs. (28) and (39). Dotted line is the Langevin function [Eq. (14)]. The inset shows corresponding differences between the Langevin function and magnetization values.

C. Cluster of uniaxial particles

One can expect that the time necessary for the cluster to reach the equilibrium magnetization value from the initial random state will increase with increasing anisotropy parameter σ . The reason is that magnetic moments of particles will have to overcome the anisotropy energy barrier. In zero magnetic field and in the absence of interactions, the characteristic time scale that determines how long it will take for the magnetic moment to overcome the barrier (i.e., to spontaneously change its orientation from \mathbf{n} to energetically equivalent $-\mathbf{n}$) is called the Néel relaxation time (τ_N). This time increases exponentially with increasing σ . With a good accuracy τ_N is given by the approximation [53]

$$\tau_N = \tau_D \frac{e^\sigma - 1}{2\sigma} \left[\frac{1}{1 + 1/\sigma} \sqrt{\frac{\sigma}{\pi}} + 2^{-\sigma-1} \right]^{-1}. \quad (40)$$

In the limit of negligible anisotropy ($\sigma \ll 1$), the Néel time τ_N reduces to the relaxation time τ_D . Equation (40) gives $\tau_N \simeq 14\tau_D$ for $\sigma = 5$, $\tau_N \simeq 6.8 \times 10^2 \tau_D$ for $\sigma = 10$, $\tau_N \simeq 5.3 \times 10^4 \tau_D$ for $\sigma = 15$, and $\tau_N \simeq 5.0 \times 10^6 \tau_D$ for $\sigma = 20$. Figure 7 demonstrates a very similar nonlinear slow down. This figure shows the dynamics of the cluster magnetization for different values of σ at a fixed field $\xi = 1$. In the beginning m_h is close to zero, but then it starts to increase and gradually reaches a nonzero equilibrium value. It is seen that as σ varies from 0 to 20, the characteristic equilibration period increases by several orders of magnitude. For larger fields ($\xi > 1$), the period decreases, but the direct simulation of clusters with $\sigma > 10$ still remains challenging from a computational viewpoint. Due to the restrictions of available computational resources, only clusters with $N = 400$ and $\sigma \leq 10$ are considered below. The integration time step is slightly increased to $\Delta t^* = 0.003$. Further increase of the time step can potentially

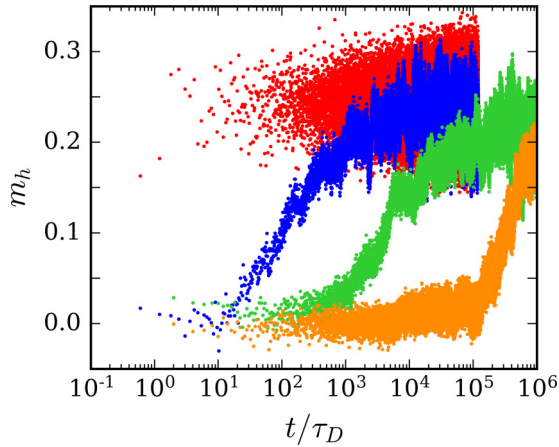


FIG. 7. Instantaneous values of the cluster normalized magnetization vs simulation time. Simulation results for $N = 400$, $\lambda = 1$, $\varphi = 0.1$, and $\xi = 1$. From top to bottom: $\sigma = 0, 10, 15$, and 20 .

lead to erroneous simulation results [25]. We use equilibration period $t^* = 500$ for $2.5 \leq \sigma \leq 7.5$ and $t^* = 4000$ for $\sigma = 10$.

Magnetization curves of a cluster of noninteracting uniaxial particles ($\lambda = 0$) were first calculated as a test. The results are given in Fig. 8. Calculations are in full agreement with Eq. (18). The linear response at weak fields is always the same as for the Langevin model, but for $\xi > 1$ the growth of $\langle m_h \rangle$ is slower the higher the anisotropy parameter σ .

Magnetization curves for clusters with $\sigma \leq 10$, $\varphi = 0.3$ and different values of λ are given in Fig. 9. The most noticeable effect of increasing anisotropy, just as in the case of noninteracting particles, is the saturation slowdown at large fields. Our phenomenological modification of MMFT given by Eq. (30) correctly reproduces this feature. As a mean-field parameter in Eq. (30), we use approximation Eq. (39) with fitting parameters previously obtained for bulk magnetoisotropic systems (see Table I). For $\lambda = 1$ [Figs. 9(a) and 9(c)], the combination of Eqs. (30) and (39) shows great quantitative

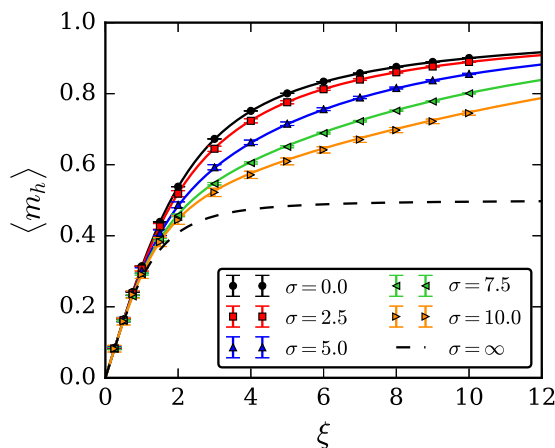


FIG. 8. Equilibrium magnetization curves of clusters of noninteracting ($\lambda = 0$) uniaxial particles. Symbols are simulation results for $N = 400$; different combinations of symbols and colors correspond to different anisotropy parameters σ (see legend). Lines are predictions of Eq. (18) for the same values of σ .

agreement with simulation data. The largest deviations are observed at intermediate fields $2 \lesssim \xi \lesssim 6$, where the analytical model overestimates the magnetization of simulated clusters. For $\sigma = 10$, the largest deviation is ≈ 0.03 . Deviations become more pronounced at $\lambda = 3$ [Figs. 9(b) and 9(d)]. At $\sigma = 10$, the largest deviation is now ≈ 0.07 . Besides, at $\lambda = 3$ and $\xi \gtrsim 10$, calculated magnetizations become larger than predictions of the analytical model. Figures 9(c) and 9(d) additionally demonstrate the predictions of “anisotropic generalizations” of MMFT1 and MMFT2. For MMFT1, this is simply a combination of Eqs. (26) and (30). For MMFT2, the mean-field parameter Eq. (27) was modified using the same intuitive approach, which was used to obtain Eq. (30)—the function $\mathcal{L}(\xi)$ was replaced with $\mathcal{L}_{\text{ani}}(\xi, \sigma)$:

$$\mathcal{C}_{mf}(\xi, \sigma) = \chi_L \left(1 + \frac{\chi_L}{16} \frac{\partial \mathcal{L}_{\text{ani}}(\xi, \sigma)}{\partial \xi} \right). \quad (41)$$

It is seen that “generalized” MMFTs overestimate calculated magnetizations at all field values starting from $\xi \simeq 2$. Just like in Sec. III B, the predictions of MMFT2 only slightly exceed the predictions of MMFT1.

IV. CONCLUSIONS

In this work, equilibrium magnetization curves of a random quasispherical cluster of single-domain nanoparticles are studied numerically and analytically. Langevin dynamics simulations show that, due to dipole-dipole interactions between particles, magnetization of the cluster is generally lower than predicted by the classical Langevin model. This is in full agreement with recent findings of Refs. [11,25]. It is shown that, in the case of negligible magnetic anisotropy and weak applied fields, magnetization curves can be successfully described by the so-called modified mean-field theory, initially proposed for the description of concentrated ferrofluids. However, as the field increases, the theory starts to overestimate the cluster magnetization. The discrepancy can be minimized by adjusting the mean-field parameter of MMFT, so that it decreases with increasing applied field. The explicit form of the dependency between the mean-field parameter \mathcal{C}_{mf} and the Langevin parameter ξ (which determines the impact of the applied field on the system) turns out to be different for different values of the dipolar coupling parameter λ and the particle volume fraction φ . For some specific combinations of λ and φ , dependencies $\mathcal{C}_{mf} = \mathcal{C}_{mf}(\xi)$ are obtained in the form of approximation formulas. Clearly, finding a universal dependency $\mathcal{C}_{mf} = \mathcal{C}_{mf}(\xi, \lambda, \varphi)$ would be useful from a practical point of view, but this requires a rigorous statistical mechanical treatment of the problem, which is beyond the scope of this work.

It is also shown that if particles have non-negligible anisotropy (characterized by the anisotropy parameter σ) and the distribution of their easy axes is random and uniform, then, at given values of ξ , λ , and φ , the magnetization of the cluster decreases with increasing σ . The decrease is much stronger at large fields. For weak dipolar coupling ($\lambda \simeq 1$), this effect can be accurately taken into account simply by replacing all Langevin functions $\mathcal{L}(\xi)$ in the magnetization expression given by MMFT [Eq. (28)] with its generalization $\mathcal{L}_{\text{ani}}(\xi, \sigma)$ [Eq. (18)]. Function $\mathcal{L}_{\text{ani}}(\xi, \sigma)$ is the exact solution for

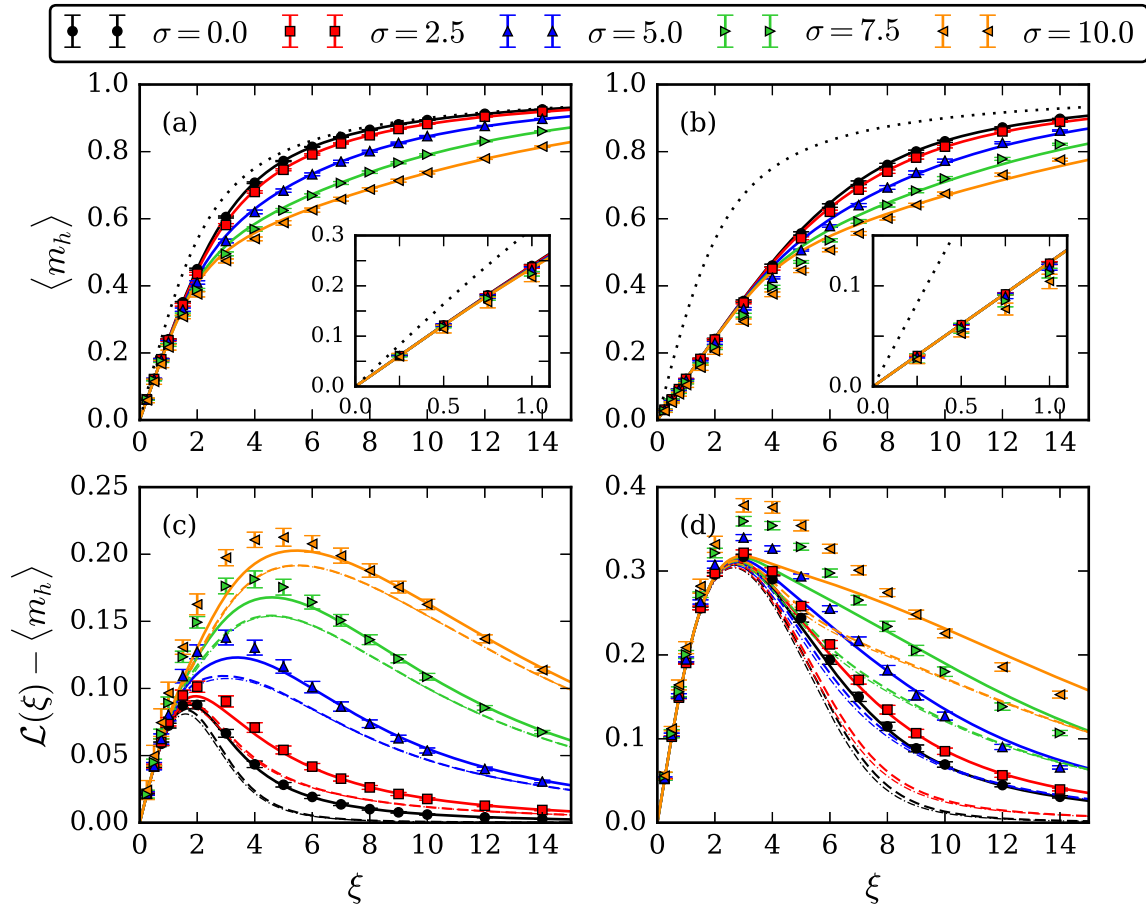


FIG. 9. Equilibrium magnetization curves of clusters with $\varphi = 0.3$. $\lambda = 1$ (a) and 3 (b). Symbols are the simulation results for $N = 400$, different combinations of symbols and colors correspond to different anisotropy parameters σ (see legend). Solid curves are predictions of the analytical model given by Eqs. (30) and (39) for the same values of σ . Dotted lines are from the Langevin model Eq. (14). Insets in (a) and (b) zoom on the weak field region. Figures (c) and (d) show differences between the Langevin function and the magnetization values shown in (a) and (b); (c) corresponds to (a) (i.e., to $\lambda = 1$) and (d) corresponds to (b) (i.e., to $\lambda = 3$). Dashed lines in (c) and (d) correspond to the analytical model given by Eqs. (26) and (30); dot-dashed lines correspond to the analytical model given by Eqs. (30) and (41).

magnetization of noninteracting uniaxial particles with random orientation texture. At larger coupling parameters ($\lambda > 1$), such a simple approach demonstrates noticeable quantitative deviations from the simulation results.

In this work, only monodisperse systems are considered. But it is known that magnetization of rigid clusters can also be influenced by the polydispersity of particles [11]. The combined effect of magnetic anisotropy, interparticle interactions,

and polydispersity on static magnetization curves of finite-size quasispherical clusters will be considered in future papers.

ACKNOWLEDGMENTS

The work was supported by Russian Science Foundation (Project No. 17-72-10033). The author is grateful to Prof. A. F. Pshenichnikov for valuable discussions.

- [1] M. A. M. Gijs, Magnetic bead handling on-chip: new opportunities for analytical applications, *Microfluid. Nanofluid.* **1**, 22 (2004).
- [2] A. Yu. Gervald, I. A. Gritskova, and N. I. Prokopov, Synthesis of magnetic polymeric microspheres, *Russ. Chem. Rev.* **79**, 219 (2010).
- [3] K. E. McCloskey, J. J. Chalmers, and M. Zborowski, Magnetic cell separation: characterization of magnetophoretic mobility, *Anal. Chem.* **75**, 6868 (2003).
- [4] S. S. Leong, S. P. Yeap, and J. Lim, Working principle and application of magnetic separation for biomedical diagnostic

- at high-and low-field gradients, *Interface Focus* **6**, 20160048 (2016).
- [5] K. J. Widder, A. E. Senyei, and D. G. Scarpelli, Magnetic microspheres: a model system for site specific drug delivery in vivo, *Proc. Soc. Exp. Biol. Med.* **158**, 141 (1978).
- [6] S. Dutz, M. E. Hayden, A. Schaap, B. Stoeber, and U. O. Häfeli, A microfluidic spiral for size-dependent fractionation of magnetic microspheres, *J. Magn. Magn. Mater.* **324**, 3791 (2012).
- [7] F. Amblard, B. Yurke, A. Pargellis, and S. Leibler, A magnetic manipulator for studying local rheology and micromechanical

- properties of biological systems, *Rev. Sci. Instrum.* **67**, 818 (1996).
- [8] M. M. van Oene, L. E. Dickinson, F. Pedaci, M. Köber, D. Dulin, J. Lipfert, and N. H. Dekker, Biological Magnetometry: Torque on Superparamagnetic Beads in Magnetic Fields, *Phys. Rev. Lett.* **114**, 218301 (2015).
- [9] C. Yang, G. Wang, Z. Lu, J. Sun, J. Zhuang, and W. Yang, Effect of ultrasonic treatment on dispersibility of Fe₃O₄ nanoparticles and synthesis of multi-core Fe₃O₄/SiO₂ core/shell nanoparticles, *J. Mater. Chem.* **15**, 4252 (2005).
- [10] S. Dutz, J. H. Clement, D. Eberbeck, T. Gelbrich, R. Hergt, R. Müller, J. Wotschadlo, and M. Zeisberger, Ferrofluids of magnetic multicore nanoparticles for biomedical applications, *J. Magn. Magn. Mater.* **321**, 1501 (2009).
- [11] V. Schaller, G. Wahnström, A. Sanz-Velasco, P. Enoksson, and C. Johansson, Monte carlo simulation of magnetic multi-core nanoparticles, *J. Magn. Magn. Mater.* **321**, 1400 (2009).
- [12] S. Dutz, Are magnetic multicore nanoparticles promising candidates for biomedical applications? *IEEE Trans. Magn.* **52**, 1 (2016).
- [13] H. Xu, Z. P. Aguilar, L. Yang, M. Kuang, H. Duan, Y. Xiong, H. Wei, and A. Wang, Antibody conjugated magnetic iron oxide nanoparticles for cancer cell separation in fresh whole blood, *Biomaterials* **32**, 9758 (2011).
- [14] S. Dutz, M. Kettering, I. Hilger, R. Müller, and M. Zeisberger, Magnetic multicore nanoparticles for hyperthermia—influence of particle immobilization in tumour tissue on magnetic properties, *Nanotechnology* **22**, 265102 (2011).
- [15] C. Blanco-Andujar, D. Ortega, P. Southern, Q. A. Pankhurst, and N. T. K. Thanh, High performance multi-core iron oxide nanoparticles for magnetic hyperthermia: microwave synthesis, and the role of core-to-core interactions, *Nanoscale* **7**, 1768 (2015).
- [16] L. Lartigue, P. Hugounenq, D. Alloyeau, S. P. Clarke, M. Lévy, J.-C. Bacri, R. Bazzi, D. F. Brougham, C. Wilhelm, and F. Gazeau, Cooperative organization in iron oxide multi-core nanoparticles potentiates their efficiency as heating mediators and MRI contrast agents, *ACS Nano* **6**, 10935 (2012).
- [17] D. Eberbeck, C. L. Dennis, N. F. Huls, K. L. Krycka, C. Gruttner, and F. Westphal, Multicore magnetic nanoparticles for magnetic particle imaging, *IEEE Trans. Magn.* **49**, 269 (2013).
- [18] V. M. Buzmakov and A. F. Pshenichnikov, On the structure of microaggregates in magnetite colloids, *J. Colloid Interface Sci.* **182**, 63 (1996).
- [19] C. Magnet, P. Kuzhir, G. Bossis, A. Meunier, L. Suloeva, and A. Zubarev, Haloing in bimodal magnetic colloids: The role of field-induced phase separation, *Phys. Rev. E* **86**, 011404 (2012).
- [20] A. S. Ivanov and A. F. Pshenichnikov, Magnetophoresis and diffusion of colloidal particles in a thin layer of magnetic fluids, *J. Magn. Magn. Mater.* **322**, 2575 (2010).
- [21] D. Borin, A. Zubarev, D. Chirikov, R. Müller, and S. Odenbach, Ferrofluid with clustered iron nanoparticles: Slow relaxation of rheological properties under joint action of shear flow and magnetic field, *J. Magn. Magn. Mater.* **323**, 1273 (2011).
- [22] Z. Guo, S. Bai, and Y. Sun, Preparation and characterization of immobilized lipase on magnetic hydrophobic microspheres, *Enzyme Microb. Technol.* **32**, 776 (2003).
- [23] V. Schaller, G. Wahnström, A. Sanz-Velasco, S. Gustafsson, E. Olsson, P. Enoksson, and C. Johansson, Effective magnetic moment of magnetic multicore nanoparticles, *Phys. Rev. B* **80**, 092406 (2009).
- [24] N. A. Usov and O. N. Serebryakova, Universal behavior of dense clusters of magnetic nanoparticles, *AIP Adv.* **6**, 075315 (2016).
- [25] P. Ilg, Equilibrium magnetization and magnetization relaxation of multicore magnetic nanoparticles, *Phys. Rev. B* **95**, 214427 (2017).
- [26] A. Weddemann, A. Auge, D. Kappe, F. Wittbracht, and A. Hütten, Dynamic simulations of the dipolar driven demagnetization process of magnetic multi-core nanoparticles, *J. Magn. Magn. Mater.* **322**, 643 (2010).
- [27] P. V. Melenev, R. Perzynski, Y. L. Raikher, and V. V. Rusakov, Monte carlo model for the dynamic magnetization of microspheres, *Phys. Procedia* **9**, 54 (2010).
- [28] N. A. Usov, O. N. Serebryakova, and V. P. Tarasov, Interaction effects in assembly of magnetic nanoparticles, *Nanoscale Res. Lett.* **12**, 489 (2017).
- [29] B. Huke and M. Lücke, Magnetic properties of colloidal suspensions of interacting magnetic particles, *Rep. Prog. Phys.* **67**, 1731 (2004).
- [30] A. F. Pshenichnikov, V. V. Mekhonoshin, and A. V. Lebedev, Magneto-granulometric analysis of concentrated ferroc colloids, *J. Magn. Magn. Mater.* **161**, 94 (1996).
- [31] A. O. Ivanov and O. B. Kuznetsova, Magnetic properties of dense ferrofluids: an influence of interparticle correlations, *Phys. Rev. E* **64**, 041405 (2001).
- [32] A. O. Ivanov, S. S. Kantorovich, E. N. Reznikov, C. Holm, A. F. Pshenichnikov, A. V. Lebedev, A. Chremos, and P. J. Camp, Magnetic properties of polydisperse ferrofluids: A critical comparison between experiment, theory, and computer simulation, *Phys. Rev. E* **75**, 061405 (2007).
- [33] Z. Wang, C. Holm, and H. W. Müller, Molecular dynamics study on the equilibrium magnetization properties and structure of ferrofluids, *Phys. Rev. E* **66**, 021405 (2002).
- [34] A. F. Pshenichnikov and V. V. Mekhonoshin, Equilibrium magnetization and microstructure of the system of superparamagnetic interacting particles: numerical simulation, *J. Magn. Magn. Mater.* **213**, 357 (2000).
- [35] R. E. Rosensweig, Heating magnetic fluid with alternating magnetic field, *J. Magn. Magn. Mater.* **252**, 370 (2002).
- [36] C. P. Bean and J. D. Livingston, Superparamagnetism, *J. Appl. Phys.* **30**, S120–S129 (1959).
- [37] Y. L. Raikher, The magnetization curve of a textured ferrofluid, *J. Magn. Magn. Mater.* **39**, 11 (1983).
- [38] R. W. Chantrell, N. Y. Ayoub, and J. Popplewell, The low field susceptibility of a textured superparamagnetic system, *J. Magn. Magn. Mater.* **53**, 199 (1985).
- [39] H. D. Williams, K. O'Grady, M. E. Hilo, and R. W. Chantrell, Superparamagnetism in fine particle dispersions, *J. Magn. Magn. Mater.* **122**, 129 (1993).
- [40] H. Mamiya and I. Nakatani, Magnetization curve for iron-nitride fine particle system with random anisotropy, *IEEE Trans. Magn.* **34**, 1126 (1998).
- [41] P. J. Clegg and L. Bessais, Series expansions for the magnetization of a solid superparamagnetic system of noninteracting particles with anisotropy, *J. Magn. Magn. Mater.* **202**, 554 (1999).

- [42] R. I. Joseph and E. Schlömann, Demagnetizing field in nonellipsoidal bodies, *J. Appl. Phys.* **36**, 1579 (1965).
- [43] C. Kittel, *Introduction to Solid State Physics* (Wiley, New York, 2004).
- [44] A. O. Tsebers, Thermodynamic stability of magnetofluids, *Magneto hydrodynamics* **18**, 137 (1982).
- [45] H. Zhang and M. Widom, Spontaneous magnetic order in random dipolar solids, *Phys. Rev. B* **51**, 8951 (1995).
- [46] D. Wei and G. N. Patey, Orientational Order in Simple Dipolar Liquids: Computer Simulation of a Ferroelectric Nematic Phase, *Phys. Rev. Lett.* **68**, 2043 (1992).
- [47] S. H. L. Klapp and G. N. Patey, Ferroelectric order in positionally frozen dipolar systems, *J. Chem. Phys.* **115**, 4718 (2001).
- [48] A. O. Ivanov, Z. Wang, and C. Holm, Applying the chain formation model to magnetic properties of aggregated ferrofluids, *Phys. Rev. E* **69**, 031206 (2004).
- [49] J. L. García-Palacios and F. J. Lázaro, Langevin-dynamics study of the dynamical properties of small magnetic particles, *Phys. Rev. B* **58**, 14937 (1998).
- [50] Z. Wang and C. Holm, Estimate of the cutoff errors in the ewald summation for dipolar systems, *J. Chem. Phys.* **115**, 6351 (2001).
- [51] E. A. Elfimova, A. O. Ivanov, and P. J. Camp, Theory and simulation of anisotropic pair correlations in ferrofluids in magnetic fields, *J. Chem. Phys.* **136**, 194502 (2012).
- [52] Z. Wang, C. Holm, and H. W. Müller, Boundary condition effects in the simulation study of equilibrium properties of magnetic dipolar fluids, *J. Chem. Phys.* **119**, 379 (2003).
- [53] W. T. Coffey, P. J. Cregg, D. S. F. Crothers, J. T. Waldron, and A. W. Wickstead, Simple approximate formulas for the magnetic relaxation time of single domain ferromagnetic particles with uniaxial anisotropy, *J. Magn. Magn. Mater.* **131**, L301 (1994).